A Survey Of Asymptote-Defined Mars Orbit Planes Supporting Interplanetary Crew Logistics

Daniel R. Adamo[1]
Astrodynamics Consultant, Salem, Oregon 97306

As of late 2016, multiple mission concepts involving humans in Mars orbit have been proposed. In virtually all these concepts, an interplanetary transport arrives in orbit about Mars, where it remains while humans explore Mars remotely, conduct sorties to one or both martian moons, or land on the planet's surface. Human operations near Mars are completed when Earth return is initiated from Mars orbit with all explorers aboard the transport. This paper surveys geometries imposed on a Mars orbit required to connect with interplanetary trajectories such that no propulsive planar steering losses are necessary at arrival and departure. By conducting this survey over a 15-year interval spanning a full cycle of Earth departures for Mars during all Earth's seasons, a broad spectrum of Mars orbit planar geometries is encountered for an interplanetary transport. Mission architectures must be adequately robust to address all these geometries, or gaps in flight opportunities exceeding 4 years will develop.

I. Nomenclature

CSP = celestial sphere plot of δ versus α
H = height above a planet's equatorial radius
HSF = human spaceflight
$\boldsymbol{I}$ = MCI unit vector directed at $\alpha = 0$; $\delta = 0$ in the Mars equatorial plane
$\boldsymbol{J}$ = MCI unit vector directed at $\alpha = +90°$; $\delta = 0$ in the Mars equatorial plane
J2K = Earth mean equator and equinox of epoch J2000.0 coordinate system
$\boldsymbol{K}$ = MCI unit vector directed at $\delta = +90°$, the Mars north celestial pole
LPIP = locus of possible injection points
MCI = Mars-centered inertial coordinate system
MOI = Mars orbit insertion impulse
TEI = trans-Earth injection impulse
$\boldsymbol{W}$ = unit vector normal to asymptote-defined Mars orbit plane
b = hyperbolic semi-minor axis
i = orbit inclination with respect to the Mars equatorial plane (MCI's $\boldsymbol{I}/\boldsymbol{J}$ plane)
r_C = circular orbit radius
r_P = planet-centered periapsis distance
t = epoch at which the MCI coordinate system is defined
$\boldsymbol{v}_\infty$ = planet-centered asymptotic velocity at a terminus in a heliocentric trajectory connecting Earth and Mars
v_∞ = planet-centered asymptotic speed at a terminus in a heliocentric trajectory connecting Earth and Mars
$\Delta\alpha$ = α shift from Mars arrival asymptote to Mars departure asymptote antipode in a specific Mars mission
Δt = time interval between two events
Δv = change-in-velocity magnitude
α = MCI right ascension, where $-180° \le \alpha \le +180°$
β = hyperbolic asymptote angle (angle between an hyperbola's asymptote and its major axis)
δ = MCI declination, where $-90° \le \delta \le +90°$
δ_∞ = MCI declination for a Mars arrival or departure asymptote
μ = Mars reduced mass = 42,828.3 km^3/s^2 [1]
θ = interplanetary trajectory heliocentric transfer angle from departure terminus to arrival terminus

[1] Sole Proprietor, 8119 Kloshe Ct. S, adamod@earthlink.net, AIAA Senior Member and Distinguished Lecturer.

II. Introduction

The vast majority of proposed architectures enabling human spaceflight (HSF) to locations on or near Mars involves an interplanetary transport in Mars orbit.[2] This transport may be prepositioned and dedicated to human occupancy only during Earth return, or it may be occupied for both outbound and return interplanetary transits. The transport's Mars orbit may be elliptical with a period of days or nearly circular with a period of hours. Unless special constraints are applied, the transport's Mars orbit plane at arrival will require adjustment prior to initiating departure for Earth. Additional planar adjustments may be required for the transport to provide human access to the surface of Mars or to its moons Phobos and Deimos in their nearly equatorial orbits. Specialized staged vehicles are typically utilized in HSF between the interplanetary transport and the Mars surface or moons, and complex architecture-specific systems trade studies are necessary to determine how much of the orbit plane change burden is assumed by a presumably more massive transport and a more nimble staged vehicle.

Assuming the interplanetary human transport is equipped with high-thrust propulsion, Earth departure opportunities for Mars will arise at intervals averaging about 26 months over time. Chiefly because Mars has a heliocentric orbit with eccentricity 0.093 and inclination 1.85° with respect to Earth's heliocentric orbit plane, the ecliptic, [2, p. 704] geometry associated with opportunities to depart Earth for Mars (and corresponding Earth returns from Mars) can vary considerably. A reasonably comprehensive survey of these variations can be performed by assessing eight successive roundtrip opportunities from Earth to Mars spanning (8 - 1)*26/12 = 15 years, the *synodic cycle* between these planets [3, p. 21]. In this manner, the sequence of eight Earth departure dates shifts later by about 12/7 = 1.7-month increments in a terrestrial calendar to sample all Earth heliocentric positions at approximately 360/7 = 51° intervals in advancing ecliptic longitude. With most Mars HSF proposals focused on initial missions in the 2030s, this paper's survey surveys a synodic cycle with Earth departures starting in 2031 and ending in 2046.

Published Mars HSF mission designs rarely account for propulsive costs required to manage an interplanetary transport's orbit plane at Mars arrival, during proximal Mars operations, and at Mars departure. Hopkins and Pratt consider a single mission case and estimate Mars orbit planar propulsion requirements for Mars arrival on 4 November 2033 [4, Section IV, Subsection B]. Adamo and Logan account for planar costs associated with Mars arrival on 30-31 March 2023 [5, p. 163], Mars departure on 8-9 August 2024 [5, p. 166], and Mars arrival on 29 June 2027 [5, p. 170]. But the author cannot cite any comprehensive survey of Mars orbit planar geometries spanning a complete synodic cycle. This paper aims to fill that void and thereby convey an appreciation for propulsive requirements necessary to address Mars orbit plane management regardless of Earth departure date.

III. Heliocentric Conic Earth to Mars Roundtrip Mission Profiles

Major influences on interplanetary transport Mars orbit geometry are exerted by each hyperbolic trajectory asymptotic velocity $\boldsymbol{v}_\infty$ with which the transport arrives and departs Mars. In accord with patched conic approximations [6, Section 6.1], these velocities are accurately determined from heliocentric conic trajectory Lambert solutions [7, Section 6.7] connecting Earth and Mars. For this synodic cycle survey, the following assumptions govern selection of Lambert solutions defining each transport mission's interplanetary trajectories.

A01: only prograde[3] *short way* Lambert solutions, each with heliocentric transfer angle $0 < \theta < 180°$, are considered. These trajectories have the shortest interplanetary transit times and therefore tend to minimize human exposure to ionizing radiation aboard the transport.

A02: a *conjunction class* flight profile, in which humans spend about 500 days exploring in the vicinity of Mars while awaiting initiation of Earth return, is adopted for each mission.

A03: consistent with A01 and A02, asymptotic speed v_∞ associated with a planetary departure or arrival is minimized to the greatest extent possible. In most prograde short way Lambert solutions connecting Earth

[2] A recent notable exception to architectures requiring an interplanetary human transport in Mars orbit is outlined in the SpaceX announcement at 2016's International Astronautical Congress (reference http://www.theverge.com/2016/9/27/13067376/elon-musk-spacex-mars-event-watch-live-stream-schedule-iac-2016, accessed 31 October 2016).

[3] In this heliocentric context, "prograde" means motion whose rotation vector (according to the right-hand rule) lies in the same hemisphere as does the rotation vector for Earth's orbit motion directed at the north ecliptic pole. Ecliptic latitude is positive for positions in the prograde hemisphere. When context shifts to Mars-centered orbits, prograde implies motion whose rotation vector lies in the same hemisphere as does the rotation vector of Mars axial rotation directed at the Mars north celestial pole.

and Mars, a conflict develops between minimizing v_∞ at both arrival and departure. In these conflicted cases, a notional compromise is made such that both v_∞ values are near their local minima.[4]

A04: at Earth arrival, the constraint $v_\infty < 4.621$ km/s is imposed. In this manner, a human-occupied vehicle returning from a conjunction class mission to Mars is subject to limited thermal and mechanical loads by ensuring direct atmospheric entry is at inertial speeds less than 12 km/s [3, p. 30].

Table 1 summarizes event timelines for the missions assessed by this paper. Planet-centered arrival and departure asymptotic speeds for each mission appear in Table 2. As a graphic example of interplanetary Lambert solutions being assessed by this paper, heliocentric inertial motion of Earth, Mars, and the interplanetary transport during Mission #1's Earth-to-Mars transit is plotted in Figure 1. A similar plot for Mission #1's Mars-to-Earth transit appears in Figure 2.

Table 1. Planetary departure and arrival dates, interleaved with tallies of the days between these dates, are listed for each of the eight missions assessed by this paper's survey.

Mission #	Depart Earth	Δt (days)	Arrive Mars	Δt (days)	Depart Mars	Δt (days)	Arrive Earth
1	2031 Feb 19	210	2031 Sep 17	511	2033 Feb 09	220	2033 Sep 17
2	2033 May 02	160	2033 Oct 09	570	2035 May 02	200	2035 Nov 18
3	2035 Jun 20	192	2035 Dec 29	559	2037 Juy 10	193	2038 Jan 19
4	2037 Aug 30	192	2038 Mar 10	518	2039 Aug 10	222	2040 Mar 19
5	2039 Oct 09	213	2040 May 09	458	2041 Aug 10	262	2042 Apr 29
6	2041 Nov 09	232	2042 Jun 29	457	2043 Sep 29	253	2044 Jun 08
7	2043 Dec 10	233	2044 Juy 30	478	2045 Nov 20	232	2046 Juy 10
8	2046 Jan 20	220	2046 Aug 28	480	2047 Dec 21	241	2048 Aug 18

Table 2. Departure and arrival asymptotic speeds with respect to Earth and Mars are listed for each of the eight missions assessed by this paper's survey.

Mission #	Depart Earth v_∞ (km/s)	Arrive Mars v_∞ (km/s)	Depart Mars v_∞ (km/s)	Arrive Earth v_∞ (km/s)
1	3.763	3.871	2.447	3.600
2	3.708	3.796	2.971	3.090
3	3.216	2.771	3.785	3.937
4	4.247	3.294	3.724	3.944
5	4.439	3.715	2.975	4.090
6	4.025	3.664	3.020	4.581
7	3.401	3.922	2.985	4.618
8	3.555	4.183	2.473	4.325

[4] Note that Lambert departure and arrival epochs are incremented at 10-day intervals to create solution datasets from which A03's near-minimal v_∞ values are identified.

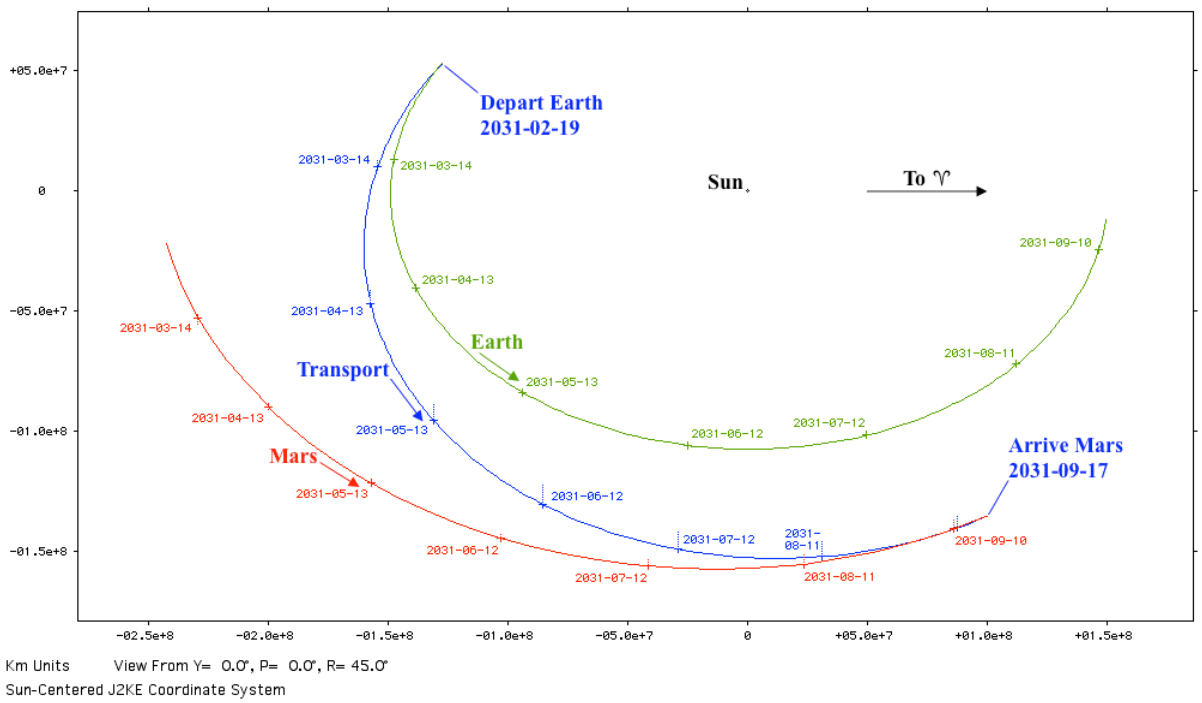

Figure 1. Mission #1 heliocentric motion of Earth (green), Mars (red), and the interplanetary transport (blue) is plotted during the transport's Earth-to-Mars transit. The direction toward zero ecliptic longitude and latitude is annotated "To ♈", and the plot is viewed from ecliptic longitude 270°; ecliptic latitude +45°. Time ticks are at 30-day intervals and annotated with calendar dates at 00:00 UT in YYYY-MM-DD format. Dotted lines from Mars and transport time ticks are projections onto the ecliptic plane.

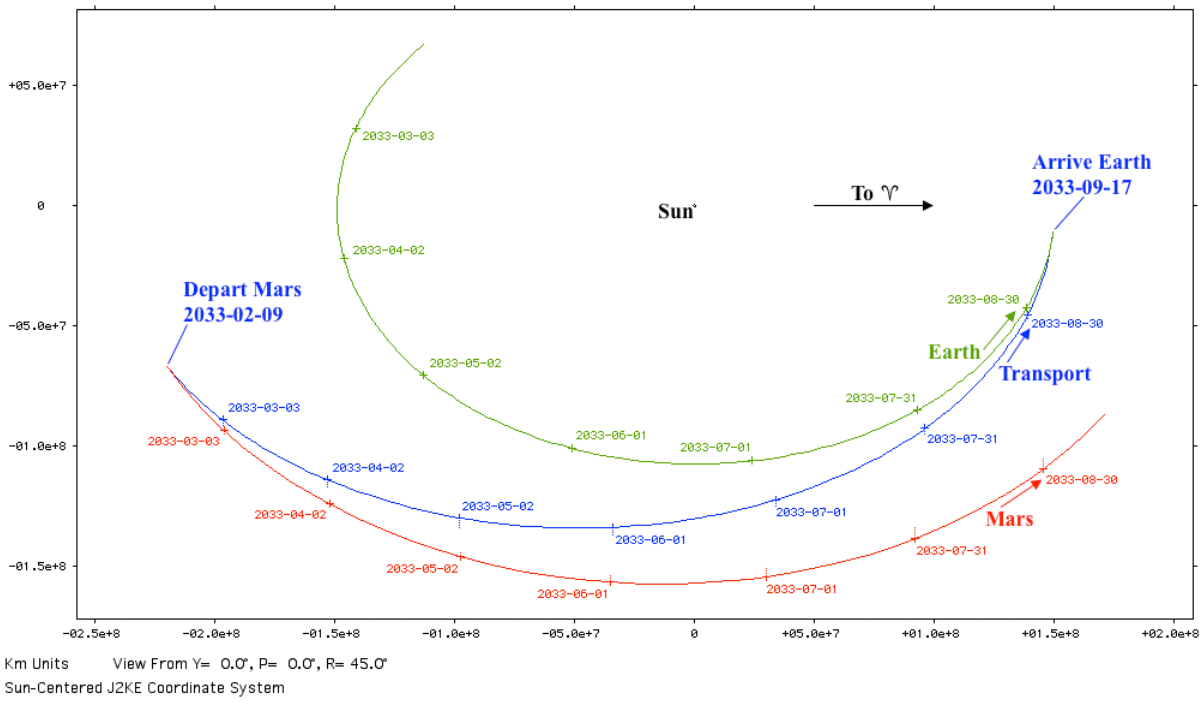

Figure 2. Mission #1 heliocentric motion of Earth (green), Mars (red), and the interplanetary transport (blue) is plotted during the transport's Mars-to-Earth transit. The direction toward zero ecliptic longitude and latitude is annotated "To ♈", and the plot is viewed from ecliptic longitude 270°; ecliptic latitude +45°. Time ticks are at 30-day intervals and annotated with calendar dates at 00:00 UT in YYYY-MM-DD format. Dotted lines from Mars and transport time ticks are projections onto the ecliptic plane.

IV. The Locus of Possible Injection Points (LPIP)

At Mars arrival, the associated $\boldsymbol{v}_\infty$ vector is the axis of symmetry for a Mars-centered small circle called the locus of possible injection points (LPIP) on which the transport's Mars orbit insertion (MOI) impulse is ideally performed to achieve orbit. Each point on the LPIP is at the periapsis distance r_P of a Mars-centered approach hyperbola. An LPIP point is unique from others on the locus only in the direction at which the LPIP is intercepted by its approach hyperbola. Assuming MOI is a purely retrograde impulse of sufficient change-in-velocity magnitude Δv, every possible post-MOI transport orbit starting at the LPIP will differ from all others only in its planar orientation. Each of these orbits will pass through the Mars approach $\boldsymbol{v}_\infty$ vector after coasting from MOI through the Mars-centered angle β, the LPIP's angular radius (β is also known as an approach hyperbola's *asymptote angle*). A value for β can be computed by first determining the hyperbolic semi-minor axis b of all approaches to the LPIP as follows [6, pp. 114-115].

$$b = r_P \sqrt{\frac{2\,\mu}{r_P\, v_\infty^{\,2}} + 1} \tag{1}$$

$$\beta = \operatorname{a\,tan}\left\{\frac{b\, v_\infty^{\,2}}{\mu}\right\} \tag{2}$$

At transport Mars departure, the associated $\boldsymbol{v}_\infty$ vector is also the axis of symmetry for a Mars-centered LPIP containing all possible trans-Earth injection (TEI) impulse locations. But the relationship between departure LPIP and $\boldsymbol{v}_\infty$ does have an important geometric distinction from the Mars approach LPIP and its $\boldsymbol{v}_\infty$. For departure, the LPIP's center lies in a Mars-centered direction *opposite* $\boldsymbol{v}_\infty$. This direction is known as the departure asymptote's *antipode*. Assuming TEI is a purely prograde impulse of sufficient Δv, every possible pre-TEI transport orbit ending at the LPIP will differ from all others only in its planar orientation. Each of these orbits will pass through the $-\boldsymbol{v}_\infty$ antipode before coasting to TEI through the Mars-centered angle β, whose value can again be computed with Equations 1 and 2.

Geocentric departure LPIPs are vividly illustrated by Brown [6, pp. 114-115]. Similar Mars-centered arrival and departure illustrations appearing subsequently in this paper assume MOI and TEI occur at r_P = 3778.1 km when evaluating Equation 1. At a Mars height H = +384.1 km, this assumption is considered safely above atmospheric entry while otherwise providing maximum efficiency for a 2-burn *Oberth sequence* to arrive at or depart from a circular transport orbit about Mars. To elaborate on such a sequence, the arrival scenario entails a retrograde MOI impulse at r_P = 3778.1 km, resulting in a Hohmann transfer to the circular orbit radius r_C. At apoapsis of the transfer, a second prograde impulse circularizes the transport's orbit.

For some r_C values near 3778.1 km, a single-burn strategy requires less total Δv than an Oberth sequence. Such an arrival scenario would entail hyperbolic approach with periapsis at r_C leading to retrograde MOI achieving the desired circular orbit. The r_C below which single-burn Δv is less than the sum of Oberth sequence impulses depends on v_∞. This paper's survey of Mars arrivals and departures is associated with the interval $2.4 < v_\infty < 4.2$ km/s as documented by Table 2. Plots of arrival/departure Δv versus r_C for both one-burn and two-burn arrivals/departures appear in Figure 3 with v_∞ = 2.4 km/s and in Figure 4 with v_∞ = 4.2 km/s.

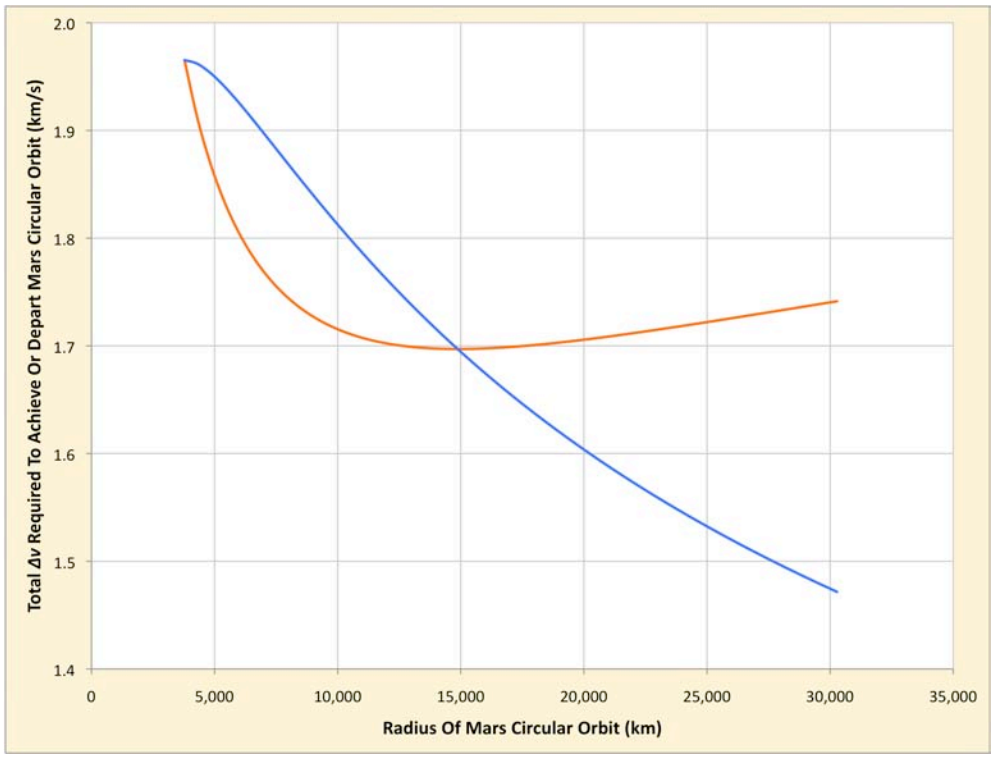

Figure 3. The Δv trade between one-burn (orange) and two-burn (blue) Mars orbit arrival/departure strategies is plotted as a function of circular orbit radius r_C when v_∞ = 2.4 km/s.

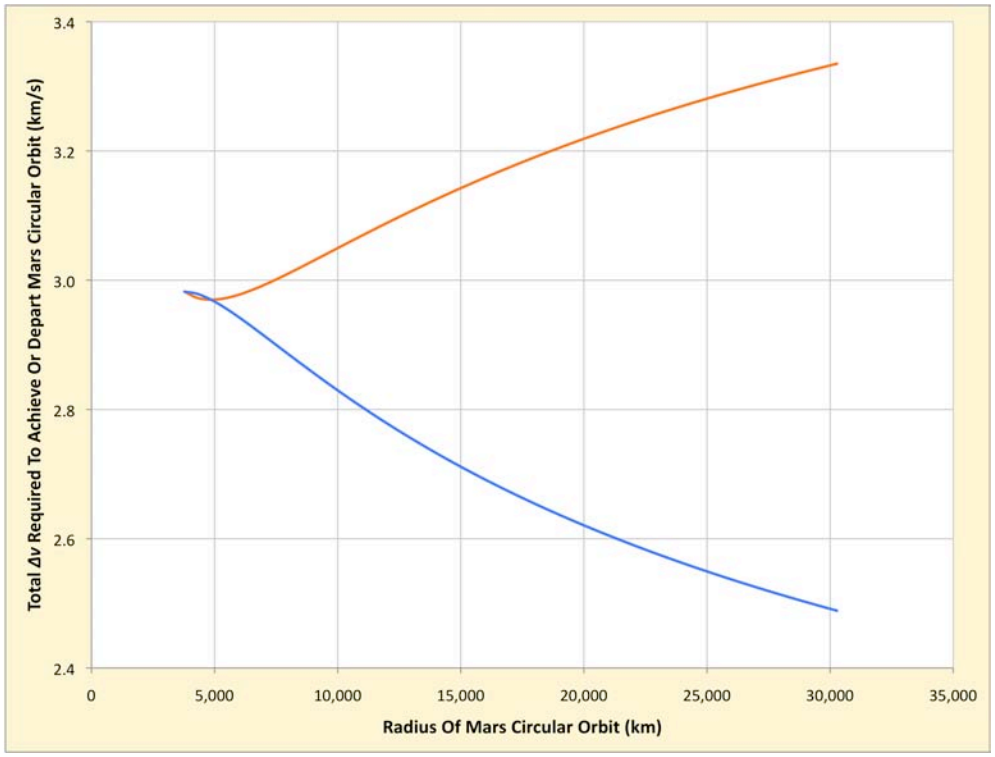

Figure 4. The Δv trade between one-burn (orange) and two-burn (blue) Mars orbit arrival/departure strategies is plotted as a function of circular orbit radius r_C when v_∞ = 4.2 km/s.

From data plotted in Figures 3 and 4, it is evident any circular transport orbit about Mars with a radius exceeding 5000 to 15,000 km will likely entail a Mars-centered hyperbolic approach from or departure to interplanetary space with an r_P near 3778.1 km[5] to maximize Oberth efficiencies. Similar conclusions can be anticipated for elliptic transport orbits about Mars, particularly those with high apoapses. Consequently, mission-specific LPIP plots appearing in Section VI are relevant to transport arrivals at and departures from a vast array of Mars-centered orbits.

V. Orbit Plane-Defining Asymptotes In The Mars-Centered Inertial (MCI) Coordinate System

Given two interplanetary transport $\boldsymbol{v}_\infty$ vectors during a particular mission, one at Mars arrival and one at Mars departure, their vector product defines the unit vector $\boldsymbol{W}$ normal to an orbit plane containing both asymptotes. Assuming no perturbations to orientation of this plane during the 500-odd days between MOI and TEI, this idealized geometry guarantees no propulsive planar steering is required for the transport at both impulses. Validity of the "no planar orbit perturbations" assumption depends primarily on apsis distances for the transport's orbit about Mars, and these apses vary considerably among Mars mission concepts. Consequently, this paper assumes constant planar orientation for the transport's Mars orbit plane to provide a reasonably insightful preliminary survey of variations in those planes over one 15-year synodic cycle.

In practice, it is highly meaningful to express Mars-centered directions in the Mars-centered inertial (MCI) coordinate system whose fundamental Cartesian axes are defined as follows at epoch t.[6]

1) $\boldsymbol{K}(t)$ is aligned with the rotation axis of Mars for epoch t using components in some standard inertial coordinate system such as the Earth mean equator and equinox of epoch J2000.0 (J2K). The $\boldsymbol{K}(t)$ direction is equivalent to MCI declination $\delta = +90°$.

2) $\boldsymbol{J}(t) = \text{unit}\left\{\boldsymbol{K}(t) \times \begin{bmatrix}1\\0\\0\end{bmatrix}\right\}$ is directed into the Mars equatorial plane, where $\delta = 0$, and at MCI right ascension $\alpha = +90°$. Note α increases in the direction of Mars rotation.

3) $\boldsymbol{I}(t) = \boldsymbol{J}(t) \times \boldsymbol{K}(t)$ to render MCI right-handed. If $\boldsymbol{I}(t)$, $\boldsymbol{J}(t)$, and $\boldsymbol{K}(t)$ are being computed with J2K components, the $\boldsymbol{K}(t)/\boldsymbol{I}(t)$ plane will contain the direction toward zero ecliptic longitude (♈) per heliocentric annotations in Figures 1 and 2. This is a consequence of using $[1, 0, 0]^T$, equivalent to the ♈ direction in J2K, when computing $\boldsymbol{J}(t)$.

One utility provided by MCI is the relation $\cos i = \boldsymbol{K}(t) \bullet \boldsymbol{W}$, where i is the transport orbit plane's inclination with respect to the Mars equatorial plane. Thus, a sufficient condition for prograde transport orbit motion is $\boldsymbol{K}(t) \bullet \boldsymbol{W} > 0$. Prograde transport motion in orbit about Mars is generally useful because it reduces Δv required for sorties between the transport and Deimos, Phobos, or the martian surface (all these destinations also exhibit prograde motion). If the vector product used to compute $\boldsymbol{W}$ results in $\boldsymbol{K}(t) \bullet \boldsymbol{W} < 0$, the order in which the two $\boldsymbol{v}_\infty$ vectors are being multiplied is simply reversed to obtain a prograde result.

Table 3 provides asymptotic declination δ_∞ values at Mars arrival and departure for each mission being assessed. These are accompanied by the shift in MCI right ascension $\Delta\alpha$ from the arrival asymptote to the departure asymptote antipode, together with i values for the asymptote-defined transport orbit plane about Mars. Note how a small $\Delta\alpha$ magnitude tends to correlate with high i.

[5] For reference, note the martian moon Phobos has a mean orbit radius of 9377.2 km, while Deimos has a mean orbit radius of 23,463.2 km [1].

[6] Note that, in order to keep a mission-specific MCI coordinate system well aligned with the equatorial plane of Mars, t is selected at the midpoint between a mission's Mars arrival and departure dates as provided in Table 1.

Table 3. Asymptotic MCI declination δ_∞ associated with Mars arrival and departure is provided for each mission surveyed. The value of each mission's MCI right ascension shift from the Mars arrival asymptote to the Mars departure asymptote antipode $\Delta\alpha$ is signed in the sense "departure minus arrival" and is positive for a prograde shift; negative for a retrograde shift. Inclination *i* for each mission's transport orbit about Mars is with respect to the martian equator.

Mission #	Mars Arrival δ_∞ (deg)	Mars Departure δ_∞ (deg)	$\Delta\alpha$ (deg)	*i* (deg)
1	+4.300	-17.920	+67.329	21.266
2	+6.137	+26.942	+95.851	28.053
3	+7.962	+25.185	+83.057	25.531
4	-10.886	+15.557	+31.535	40.934
5	-25.586	-3.980	+11.059	64.967
6	-25.787	-40.075	-18.335	52.623
7	-10.476	-43.989	-3.078	86.065
8	+5.478	-34.449	+55.810	41.973

Missions #5, #6, and #7 probably have excessive *i* in the context of sorties to Phobos ($i = 1.082°$) or Deimos ($i = 1.791°$) [1]. An interplanetary transport orbiting Mars at $i > 45°$ may also be unsuitable for human logistics to and from the martian surface. In such cases, it may be preferable to abandon the asymptote-defined transport orbit plane strategy altogether. An alternative would entail performing MOI to achieve *i* near or slightly greater than $\left|\delta_\infty\right|$ at Mars arrival. A dedicated plane change impulse would then be required to achieve *i* near or slightly greater than $\left|\delta_\infty\right|$ at Mars departure. Note none of the Table 3 arrival $\left|\delta_\infty\right|$ values exceed 26°, but departure $\left|\delta_\infty\right|$ values approach 44°.

If a dedicated transport plane change must be performed in Mars orbit, it is likely best to do so near apoapsis of an elliptical orbit where Mars-centered speed is minimal. But an elliptical orbit about Mars can introduce geometric difficulties not present in near-circular orbits. First, the line of nodes between elliptical orbits before and after a plane change must closely coincide with their respective lines of apsides, or propulsive efficiencies from a near-apoapsis plane change impulse cannot be realized. Second, periapsis of the final elliptical orbit must be near TEI's LPIP, or return to Earth cannot be initiated with adequate propulsive efficiency. Due to these difficulties, some architectures maneuver the interplanetary transport to a strategic location in Mars orbit, such as Phobos or Deimos, where Earth return consumables including propellant are cached.

Orbit geometries for Missions #1 through #8, together with the correlation between $\Delta\alpha$ magnitude and *i* in Table 3, can be visualized by application of MCI coordinates to plots of δ versus α. In this application, transport orbit planes, $\boldsymbol{v}_\infty$ vectors, and LPIPs are mapped onto a Mars-centered celestial sphere. These celestial sphere plots (CSPs) are described and illustrated for Missions #1 through #8 in the following section.

VI. Mars-Centered Inertial (MCI) Celestial Sphere Plots (CSPs)

Any Mars-centered direction can be mapped onto plots of δ versus α, a representation of the celestial sphere in MCI coordinates. When regarding such a CSP on a flat orthogonal grid, as in this section, it is important to recall directions differ from those on a conventional map of the martian surface because the celestial sphere is being viewed from its *inside*. Consequently, although MCI north[7] is upward on a CSP, MCI east[8] is *leftward* from this interior perspective. Figures 5 through 12 present CSPs for Missions #1 through #8, respectively. For reference, the direction to zero ecliptic longitude and zero ecliptic latitude on Earth's heliocentric orbit plane is indicated in each CSP with a black "+" marker annotated by "♈".

[7] The MCI north direction on a CSP is that of increasing δ.

[8] The MCI east direction on a CSP is that of increasing α.

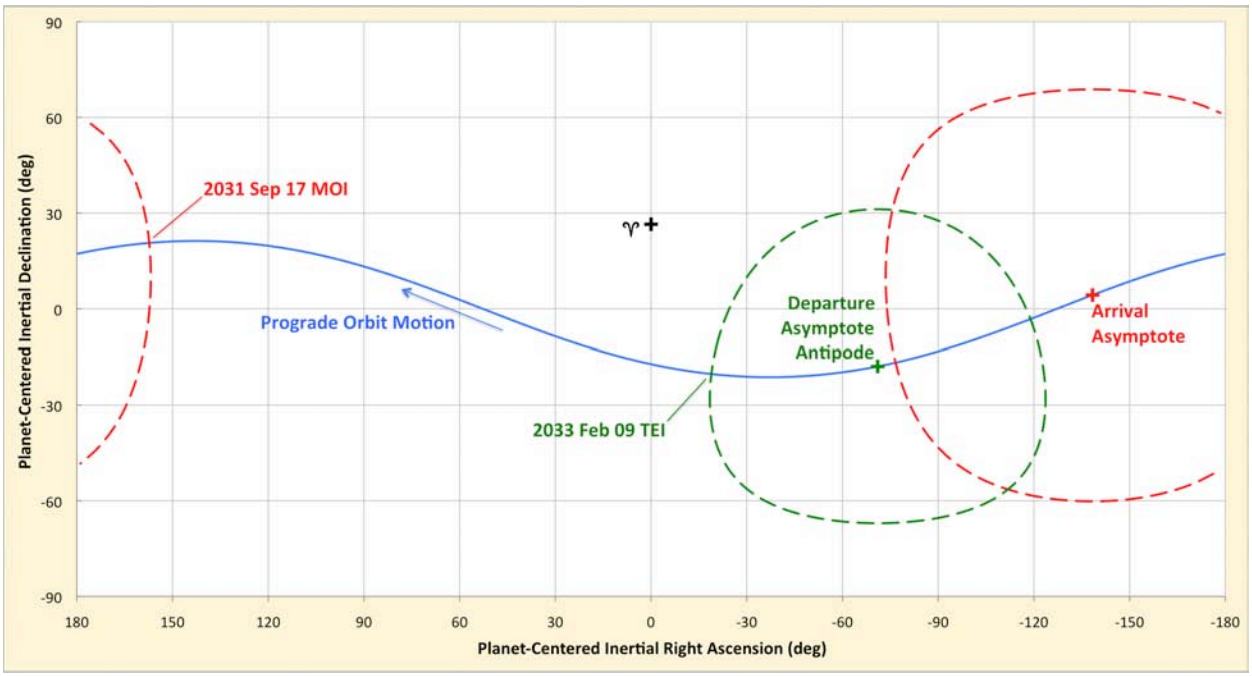

Figure 5. Mission #1's CSP illustrates the prograde orbit plane (blue) connecting Mars arrival and departure asymptotes. The dashed red curve is the LPIP for MOI, and the dashed green curve is the LPIP for TEI.

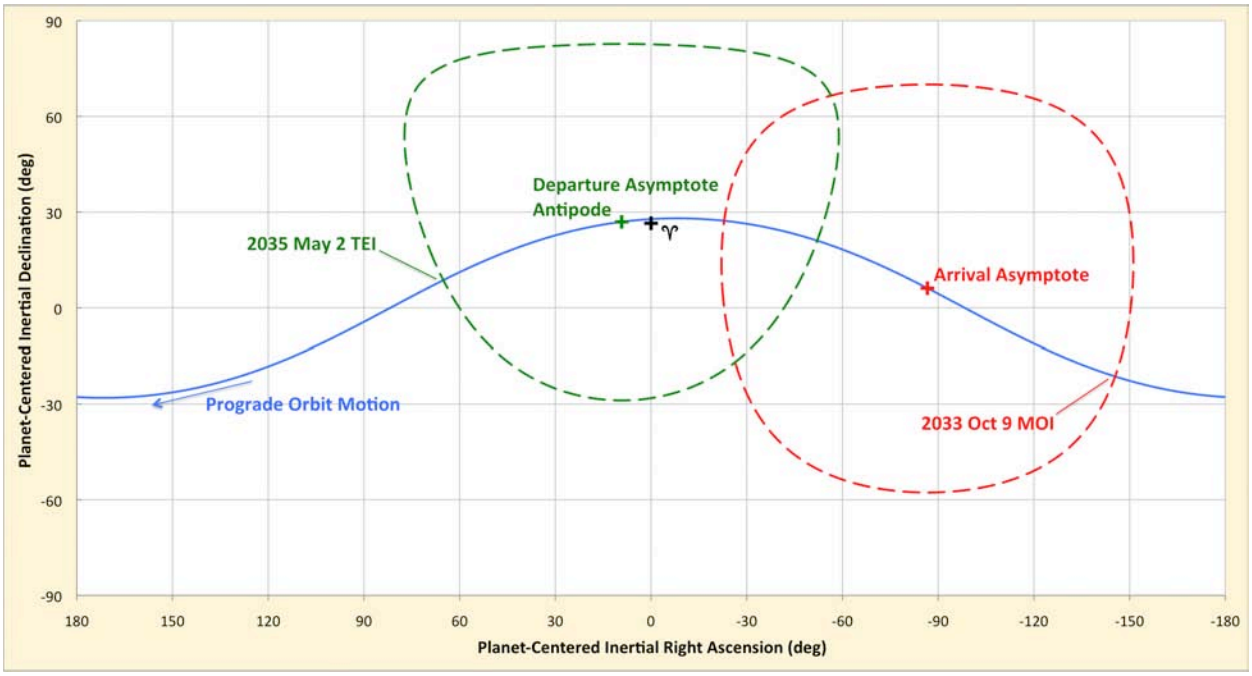

Figure 6. Mission #2's CSP illustrates the prograde orbit plane (blue) connecting Mars arrival and departure asymptotes. The dashed red curve is the LPIP for MOI, and the dashed green curve is the LPIP for TEI.

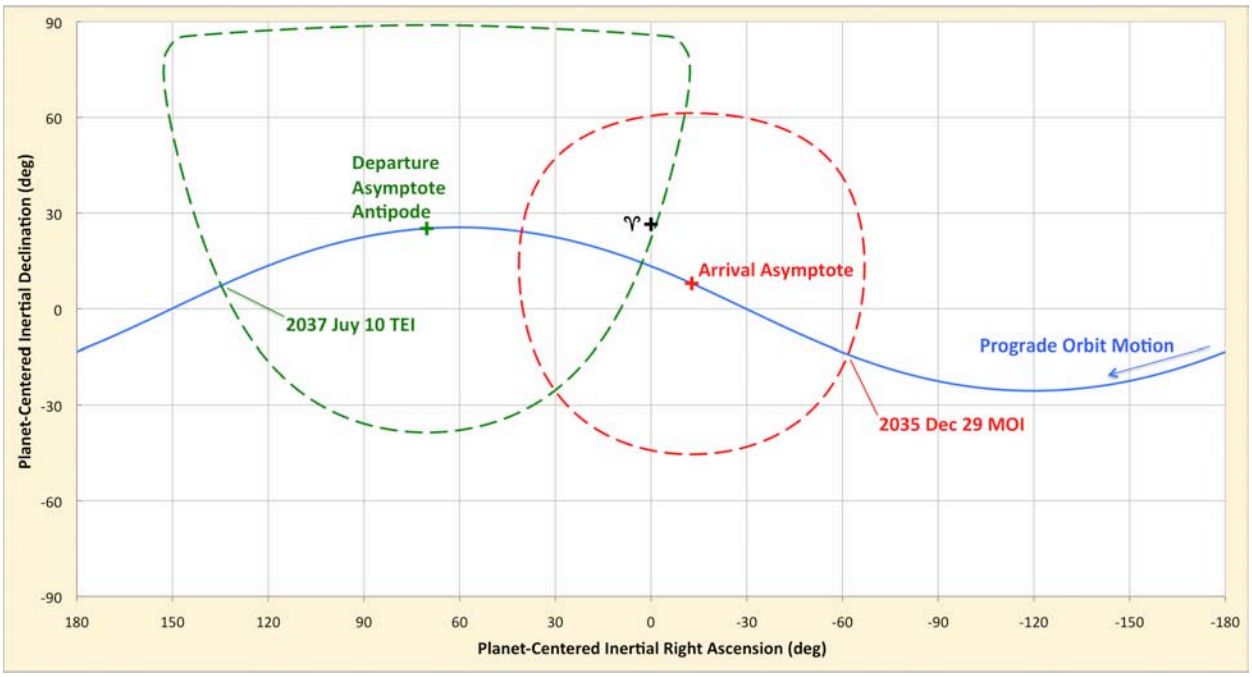

Figure 7. Mission #3's CSP illustrates the prograde orbit plane (blue) connecting Mars arrival and departure asymptotes. The dashed red curve is the LPIP for MOI, and the dashed green curve is the LPIP for TEI.

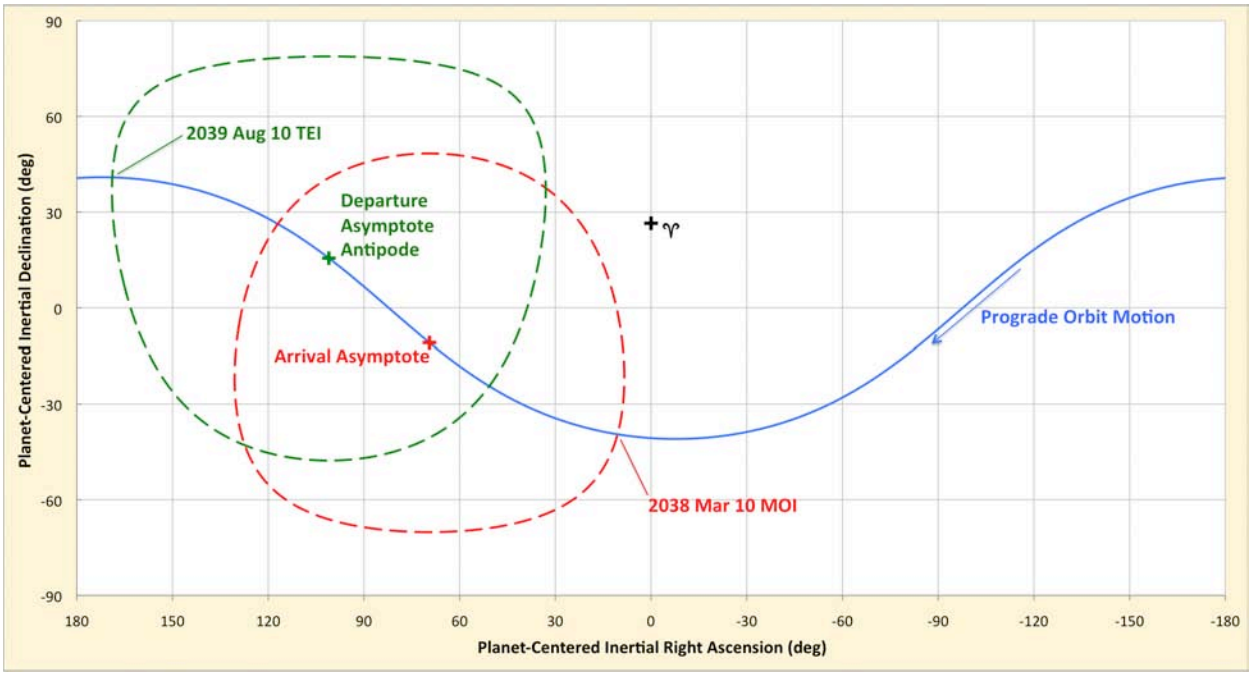

Figure 8. Mission #4's CSP illustrates the prograde orbit plane (blue) connecting Mars arrival and departure asymptotes. The dashed red curve is the LPIP for MOI, and the dashed green curve is the LPIP for TEI.

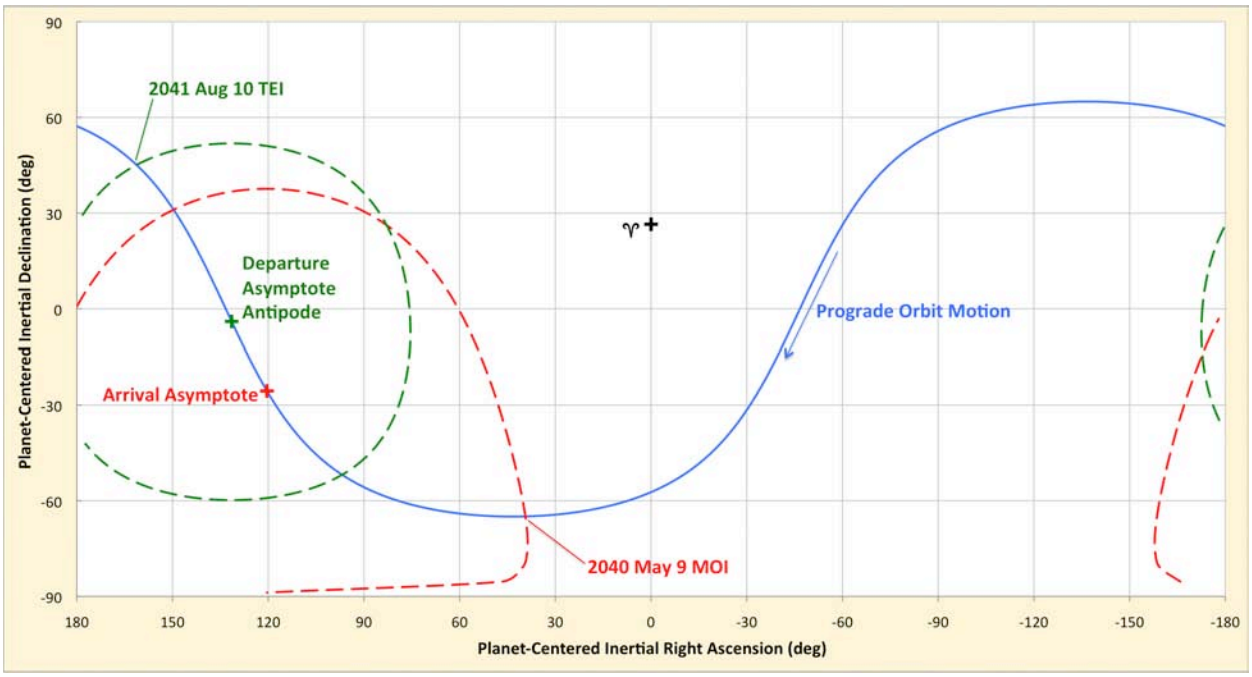

Figure 9. Mission #5's CSP illustrates the prograde orbit plane (blue) connecting Mars arrival and departure asymptotes. The dashed red curve is the LPIP for MOI, and the dashed green curve is the LPIP for TEI.

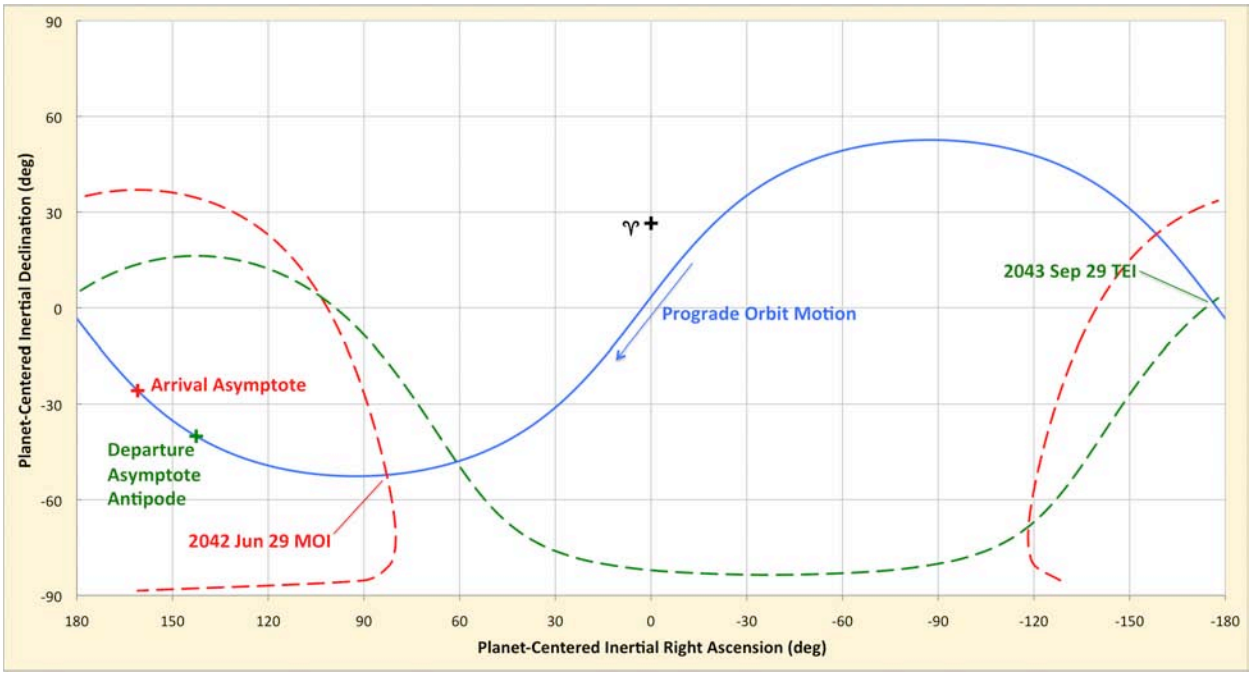

Figure 10. Mission #6's CSP illustrates the prograde orbit plane (blue) connecting Mars arrival and departure asymptotes. The dashed red curve is the LPIP for MOI, and the dashed green curve is the LPIP for TEI.

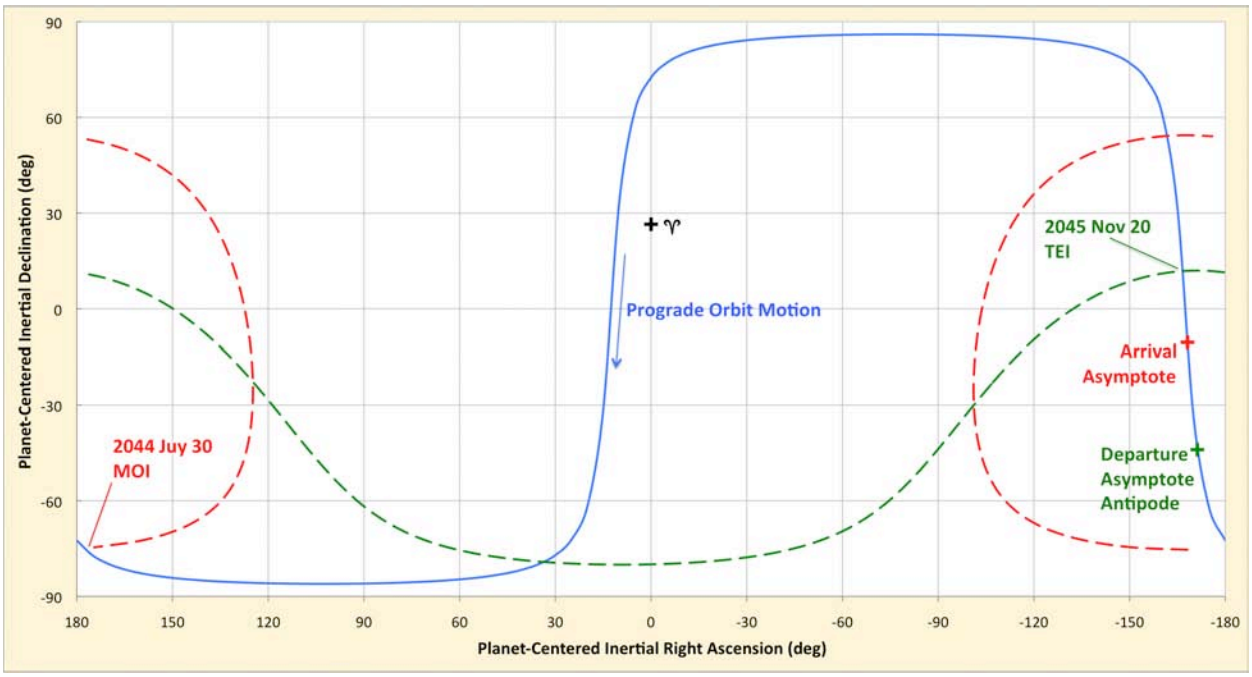

Figure 11. Mission #7's CSP illustrates the prograde orbit plane (blue) connecting Mars arrival and departure asymptotes. The dashed red curve is the LPIP for MOI, and the dashed green curve is the LPIP for TEI.

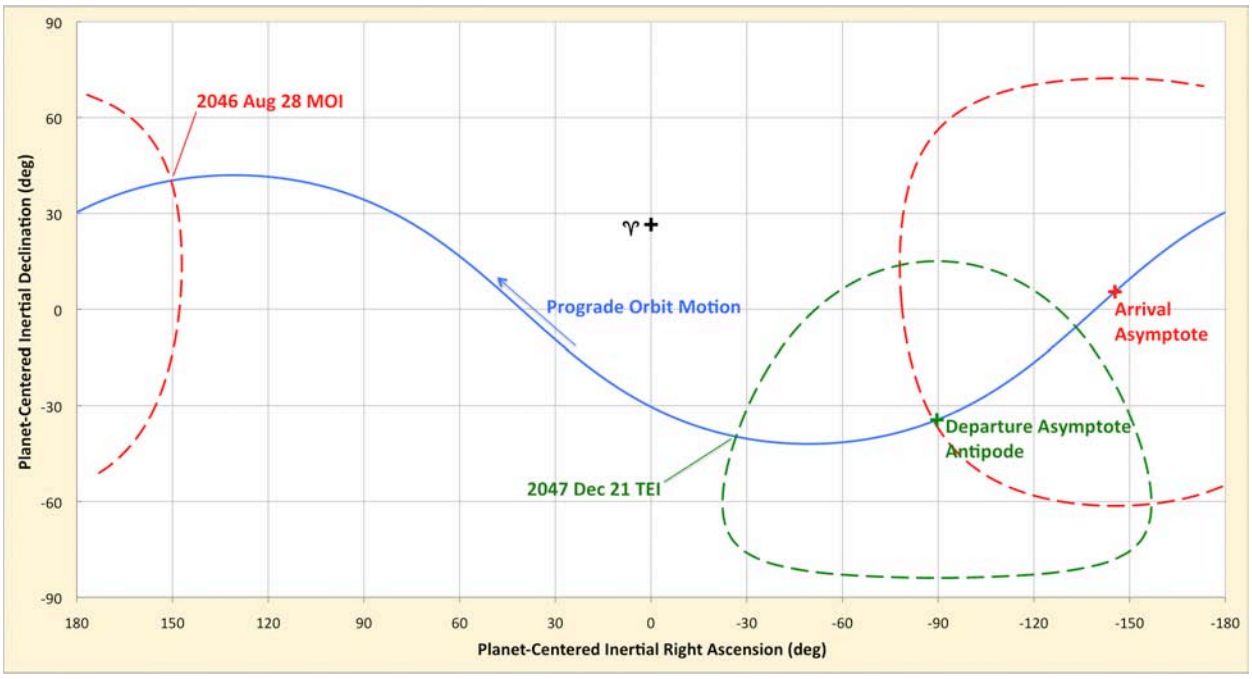

Figure 12. Mission #8's CSP illustrates the prograde orbit plane (blue) connecting Mars arrival and departure asymptotes. The dashed red curve is the LPIP for MOI, and the dashed green curve is the LPIP for TEI.

VII. Conclusion

This paper applies the simple technique of defining a human spaceflight transport's Mars orbit plane with asymptotic velocities required to arrive from and depart to Earth, while further assuming no planar perturbations between arrival and departure. This technique is assessed for eight successive mission opportunities spanning the synodic cycle of Earth departures for Mars extending from 2031 to 2046. Theoretically, such an asymptote-defined orbit plane strategy would be free of planar propulsive costs at Mars arrival and departure. A variety of Mars orbit geometries arises from this strategy, and this paper documents each in a meaningful Mars-centered inertial coordinate system. It may be necessary to depart from the asymptote-defined orbit plane for many roundtrip missions to Mars, but doing so will entail architecture-specific performance trades between the transport and any staged vehicles accessing the martian surface or moons Phobos and Deimos orbiting near the Mars equatorial plane. These specific architectures may also impose Mars orbit eccentricities and planar orientations departing from the asymptote-defined orbits assumed by this paper's survey. It may also be desirable to maneuver the transport to strategic locations, such as Phobos or Deimos, where consumables supporting Earth return have been cached.

Considerable propulsive cost may therefore be incurred in managing a specific interplanetary transport's Mars orbit plane during a specific mission opportunity. Furthermore, this cost is highly variable among Earth roundtrip mission opportunities to Mars as indicated by digital and graphic data presented in this paper. Planar management requirements reflecting pertinent orbit perturbations should consequently be assessed in any comprehensive design reference mission study whose architecture includes an interplanetary transport orbiting Mars. For elliptical transport orbits, apsidal rotation influences on orbit plane management must also be assessed. To ensure interplanetary human spaceflight architectures can address all Mars orbit geometries they encounter, at least the worst case from an entire Earth/Mars synodic cycle spanning eight successive mission opportunities must be studied in detail. Failure to account for worst-case Mars orbit planar management costs could result in programmatically undesirable mission opportunity gaps. Just a single missed opportunity will result in an interval approximately 52 months (4.3 years) between viable Mars missions.

References

[1] J. D. Giorgini, D. K. Yeomans, A. B. Chamberlin, P. W. Chodas, R. A. Jacobson, M. S. Keesey, J. H. Lieske, S. J. Ostro, E. M. Standish, R. N. Wimberly, "JPL's On-Line Solar System Data Service", *Bulletin of the American Astronomical Society*, Vol. 28, No. 3, p. 1158, 1996.[9]

[2] P. K. Seidelmann (ed.), *Explanatory Supplement to the Astronomical Almanac*, University Science Books, 1992.

[3] B. G. Drake (ed.), *Human Exploration of Mars Design Reference Architecture 5.0*, NASA/SP-2009-566, 2009.[10]

[4] J. B. Hopkins and W. D. Pratt, "Comparison of Deimos and Phobos as Destinations for Human Exploration and Identification of Preferred Landing Sites", AIAA SPACE 2011 Conference & Exposition, AIAA 2011-7140.[11]

[5] D. R. Adamo and J. S. Logan, "*Aquarius*, A Reusable Water-Based Interplanetary Human Spaceflight Transport", *Acta Astronautica*, Vol. 128, November-December 2016, pp. 160-179.[12]

[6] C. D. Brown, *Spacecraft Mission Design*, AIAA Education Series, 1992.

[7] D. A. Vallado, *Fundamentals of Astrodynamics and Applications*, McGraw-Hill, 1997.

[9] This service can be utilized at http://ssd.jpl.nasa.gov/?horizons (accessed 8 November 2016).

[10] This document may be downloaded at http://www.nasa.gov/exploration/library/esmd_documents.html (accessed 31 October 2016).

[11] This paper may be downloaded at http://www.csc.caltech.edu/references/Hopkins-Phobos-Deimos-Paper.pdf (accessed 13 November 2016).

[12] This paper may be downloaded at http://www.sciencedirect.com/science/article/pii/S0094576516300868 (accessed 13 November 2016).